Journal of Magnetism and Magnetic Materials 454 (2018) 228–236

Contents lists available at ScienceDirect

Journal of Magnetism and Magnetic Materials

journal homepage: www.elsevier.com/locate/jmmm

Research articles

Controllable oxygen vacancies, orbital occupancy and magnetic ordering in $SrCoO_{3-\delta}$ films

Youdi Gu [a,b,e], Cheng Song [b], Hongrui Zhang [c], Zechao Wang [d], Bin Cui [b], Fan Li [b], Jingjing Peng [b], Muhammad Shahrukh Saleem [b], Guangyue Wang [b], Xiaoyan Zhong [d], Fei Wang [a], Song Ma [a], Jirong Sun [c], Wei Liu [a,e,*], Feng Pan [b], Zhidong Zhang [a,e]

[a] Shenyang National Laboratory for Materials Science, Institute of Metal Research, Chinese Academy of Sciences, Shenyang 110016, China
[b] Key Laboratory of Advanced Materials (MOE), School of Materials Science and Engineering, Tsinghua University, Beijing 100084, China
[c] Beijing National Laboratory for Condensed Matter, Institute of Physics, Chinese Academy of Sciences, Beijing 100190, China
[d] National Center for Electron Microscopy in Beijing, School of Materials Science and Engineering, Tsinghua University, Beijing 100084, China
[e] University of Chinese Academy of Sciences, Beijing 100049, China

ARTICLE INFO

Article history:
Received 1 December 2017
Received in revised form 10 January 2018
Accepted 25 January 2018

Keywords:
$SrCoO_{3-\delta}$ thin films
Oxygen vacancy
Orbital occupancy
Magnetic ordering
Epitaxial strain

ABSTRACT

Epitaxial strain imposed in complex oxide ultrathin films is recognized as a powerful tool for controlling the ground state of correlated electron system. Here, we achieved simultaneous control of oxygen vacancies, orbital occupancy and magnetic ordering through the facile application of epitaxial strain, both tensile and compressive, in $SrCoO_{3-\delta}$ oxygen "sponge" material rather than the ordinary manganites. The oxygen vacancies are enhanced greatly as the strain changes from smaller tensile 1.0% to larger tensile 2.0%, then to moderate compressive -1.0% in $SrCoO_{3-\delta}$ films, associated with $3-\delta$ varying from ~2.90 to ~2.835, then to ~2.72. Highest saturated magnetization is found in the thin films in small tension on $La_{0.3}Sr_{0.7}Al_{0.65}Ta_{0.35}O_3$ substrate and lower values are found in larger tension on $SrTiO_3$ and lowest values in moderate compression on $LaAlO_3$. Meanwhile, electrons prefer to occupy the in-plan oriented orbitals for the tensile strain, in contrast to the preferential out-of-plane orbital occupancy for the compressive state associated with coupled intermediate spin-Co^{4+} ($t_{2g}^4e_g^1$)/high spin-Co^{3+} ($t_{2g}^4e_g^2$) in different proportions depending on strain states. Such controllable spin and orbital configurations lead to more robust magnetization in tensile strained $SrCoO_{3-\delta}$ films than in its compressive counterpart. Our findings provide a nostrum for tailoring and controlling new magnetic, electronic and ionically active properties with strain engineering and further enrich orbital physics in cobaltites.

1. Introduction

Disclosing and Controlling the interactions between lattice, charge, spin and orbital degrees of freedom in strong correlated transition-metal oxides is at the center of modern condensed matter physics and oxide spintronics [1–3]. In addition to these intrinsic physical factors, extrinsic oxygen vacancies can also play a crucial role in enabling novel electronic, magnetic, structural properties and newfangled functionality in transition-metal oxides and their interface [4,5]. For example, oxygen vacancies can induce ferroelectric and ferromagnetic behavior in multiferroic $SrMnO_3$ films [6,7], and an antiferromagnetic-ferromagnetic transition caused by oxygen vacancies was reported in the multiferroic $Eu_{0.5}Ba_{0.5}TiO_{3-\delta}$ films [8]; also, the oxygen vacancies ordering has been found to stabilize long-range ferromagnetic ordering in $LaCoO_{3-\delta}$ [9].

The natural oxygen "sponge" material of strontium cobaltite, with a topotactic structural phase transition from perovskite $SrCoO_{3-\delta}$ ($0 \le \delta \le 0.25$; P-SCO) to brownmillerite $SrCoO_{2.5}$ (BM-$SrCoO_{2.5}$) accompanying the magnetic phase transition from ferromagnetism to antiferromagnetism [10–12], shows potential applications in spintronics, catalytic reactions, and solid-oxide fuel cells. The complex phase diagram [13,14], rich physical properties of different phases [10,11], recently discovered electric-field controlled tri-state phase transformation [15], interesting valence and spin states [16–18], as well as reversible redox reactions through the topotactic phase transition [10,11,19,20] make strontium cobaltite recently become a potentially useful material. Very recently, the oxygen vacancies and magnetic phases of SCO films have been modulated by epitaxial tensile strain [21–23]. The bridge between the phase transition, property variation and the

---

* Corresponding author at: Institute of Metal Research, Chinese Academy of Sciences, Shenyang 110016, China.

E-mail address: wliu@imr.ac.cn (W. Liu).

https://doi.org/10.1016/j.jmmm.2018.01.083
0304-8853/© 2018 Elsevier B.V. All rights reserved.

epitaxial strain of SCO films is oxygen vacancies. They claimed that the formation energy of oxygen vacancies in SCO films is strongly favored by tensile strain. *Ab initio* calculations actually support a lowering of oxygen vacancies formation energy under tensile strain for SCO [23] and other perovskite oxides, like $SrMnO_3$ [24], $CaMnO_3$ [25,26], $SrTiO_3$ [27], or $LaAlO_3$ [28]. Nevertheless, the ability to form oxygen vacancies in SCO films under tensile and compressive strains is still an open question. For example, recent measurements in SCO thin films by Hu et al. [29] revealed that both moderate compressive and larger tensile epitaxial strain can reduce significantly the oxygen vacancies activation energy barrier in SCO. Furthermore, Cazorla et al. [30] used first-principle methods to demonstrate that it was easiest to create oxygen vacancies in -2% compressively strained SCO films. So whether the same preference for oxygen vacancies formation that have been observed in SCO films at tensile conditions may also occur at other epitaxial strains remains to be experimentally demonstrated. Moreover, it is also predicted that epitaxially strained SCO shows coupled magnetic-ferroelectric and metal-insulator transition due to the strong coupling between the lattice, electrical polarization and electronic band gap and potentially enable SCO to be a novel multiferroic material [12,21,31], which makes it even more intriguing to study the strong strain coupling of structural, ionic, electronic and magnetic properties.

It is generally accepted that the physical properties of transition metal oxides depend strongly on the occupancy of 3*d* orbits [32–35]. Most of current research on orbital physics is concentrated in manganites and nickelates. For cobaltites, possible spin and magnetic ground states have been investigated to show high spin (HS), intermediate spin (IS), and low spin (LS) states for different valence states of cobalt cations [16–18,36,37]. However, the orbital occupancy and spin states under different strain, both tensile and compressive, have not been reported in SCO films until now. In the experiments below we combine the results of X-ray absorption spectroscopy (XAS), X-ray linear dichroism (XLD), magnetization and transport measurements to investigate the oxygen vacancies, orbital occupancy, and magnetic transition in strontium cobaltite films with different strain states, providing a platform for the interactions between lattice, charge, spin, and orbital degrees of freedom.

2. Materials and methods

SCO films with 18 nm thickness were grown by pulsed laser deposition (PLD) with a KrF excimer laser from a stoichiometric $SrCoO_3$ target. The (0 0 1)-oriented $LaAlO_3$ (LAO) substrates were used for compressive strain, while $La_{0.3}Sr_{0.7}Al_{0.65}Ta_{0.35}O_3$ (LSAT) and $SrTiO_3$ (STO) were used for tensile strain. During growth, the substrates were held at 710 °C and in an oxygen background pressure of 200 mTorr. The growth was monitored *in situ* by reflection high-energy electron diffraction (RHEED) analysis allowing precise control of the thickness at the unit cell scale and accurate characterization of the growth dynamics. After growth, the samples were slowly cooled to room temperature in 600 Torr of oxygen at a rate of ~5 °C/min to improve the oxidation level after growth.

The crystal structure of the films was characterized by using a Bruker diffractometer (D8 Discover, Cu K_α radiation). The atomic resolution aberration-corrected high-angle annular dark field scanning transmission electron microscopy (HAADF-STEM) images were taken by the FEI Titan G2 80-200 CREWLEY [38]. A superconducting quantum interference device (SQUID) magnetometer was used to measure the magnetic properties of SCO films. In-plane electrical transport measurements were conducted using the patterned Hall bar devices in a Physical Property Measurement System (PPMS) in a cooling process. Cobalt $L_{2,3}$-edge XAS and XLD and oxygen *K*-edge XAS measurements were performed in total electron yield (TEY) detection mode at room temperature at Beamline BL08U1A of Shanghai Synchrotron Radiation Facility (SSRF). The cobalt $L_{2,3}$-edge spectra were normalized to the maximum intensities of L_3 peak. The XLD spectra normalization was made by dividing the spectra by a factor such that the L_3 pre-edge and L_2 post-edge have identical intensities for the two polarization. After that, the pre-edge spectral region was set to zero and the peak at the L_3 edge was set to one.

3. Results and discussions

To understand the effect of strain-induced oxygen vacancies on the electric and magnetic properties, we have grown SCO epitaxial films on three different (0 0 1)-oriented LAO, LSAT and STO substrates by PLD. The typical fine RHEED intensity oscillations were observed during the deposition of SCO films, as shown in Fig. 1(a). The initial diffraction spots of bare substrates became clear stripes [inset of Fig. 1(a)] patterns of SCO films, indicating the development of layer-by-layer growth mode. To get further information about the mode for film growth and interface structure, we performed a transmission electron microscopy analysis of the SCO films. Fig. 1(b) illustrates the representative HAADF-STEM image of the interface region for the one selected SCO/LAO film. The HADDF-STEM image shows a perfect epitaxial film growth on the substrate. The film is fully strained, and the film/substrate interface is very clear, free from obvious defects.

Fig. 1(d) shows the full spectra of X-ray diffraction (XRD) $\theta - 2\theta$ scans for the 18 nm SCO films grown on LAO, LSAT and STO substrates. Only SCO film and substrate peaks are observed, without any impurity peaks, such as half-order peaks of brownmillerite phase. Note that all the samples show (0 0 2) SCO film peaks (denoted as arrows) associated with the substrates' peaks (marked as diamonds), indicating the epitaxial growth of the SCO films [Fig. 1(e)]. The (0 0 2) SCO peaks exist at the left side of that of LAO substrate, reflecting the in-plane compressive strain in the film, while on the LSAT and STO substrates does the opposite due to the tensile strain. This finding is consistent with the lattice mismatch of -1.0%, 1.0% to 2.0% between P-SCO (3.829 Å) and the LAO, LSAT, STO substrates, respectively, as shown in Fig. 1(c). The strain states of all films were further verified by X-rays reciprocal space maps (RSMs) around the $(-1\,0\,3)$ Bragg peak positions [Fig. 1(f–h)]. The RSM is a powerful method to quantify the strain state, which can be identified by the intensity distribution in the vicinity of the detected Bragg peak. In addition to the systematic change in the out-of-plane lattice constant, the diffraction peaks of SCO films align vertically with those of the substrates, indicating a coherent strained growth for all samples. Therefore, the in-plane lattice constants of the films are identical to that of substrates.

The valence states of cobalt cations and the oxygen concentration in the SCO films were probed by XAS at the cobalt $L_{2,3}$-edge and oxygen *K*-edge. This technique provides important information on magnetic and electric properties of cobalt and cobaltites [39,40]. Corresponding data are shown in Fig. 2. In Fig. 2(a), all the cobalt $L_{2,3}$-edge XAS curves are featured as shoulder peaks on both the high and low-energy sides of the main peaks, due to spin-orbit splitting of cobalt 2*p* core hole [41]. The most eminent feature here is the shift of the L_3 peak towards to a higher photon energies direction, e.g., from ~778.48 to ~778.85 then to ~778.67 eV, with changing the strain from -1.0% to 1.0% then to 2.0%, as summarized in Fig. 2(b). A clearer shift of cobalt L_3-edge was plotted in the left side of Fig. 2(a). This observation indicates a lower valence state of cobalt cations and a higher amount of oxygen vacancies in compressive strained films. It is worth noting that

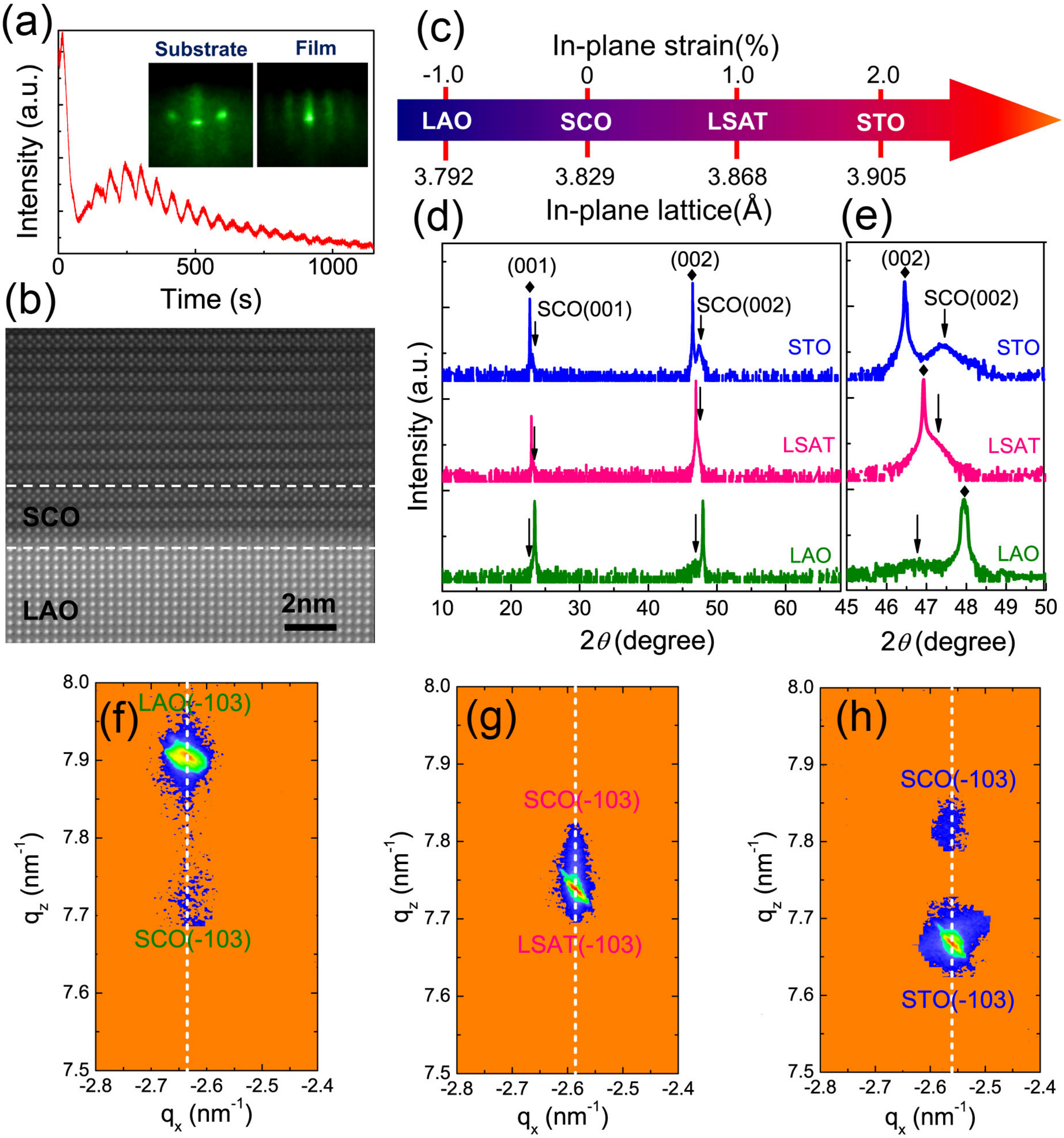

Fig. 1. Growth and structural characterization of SCO films. (a) RHEED intensity oscillations during the deposition of SCO films. The insets are RHEED patterns of bare substrates and SCO films during growth. (b) Representative HAADF-STEM image of the interface region in SCO/LAO film. (c) Schematic diagram of in-plain lattice parameters and in-plane strain between SCO and LAO, LSAT and STO substrates. (d) The full spectra of XRD $\theta - 2\theta$ scans for the SCO films grown on LAO, LSAT and STO substrates. (e) XRD $\theta - 2\theta$ scans for the SCO films around the substrate (0 0 2) peak. (The (0 0 2) Brag reflections from the SCO films and the substrates are denoted as arrows and diamonds, respectively). X-ray RSMs are shown around the (-1 0 3) Bragg peak positions from (f) LAO, (g) LSAT and (h) STO substrates.

direct growth of perovskite SCO film with fully stoichiometry ($\delta = 0$) by PLD is a very difficult task and our SCO films on LSAT substrate show the highest cobalt L_3 peak photon energies, indicating minimal oxygen vacancies and excellent quality film. This, together with clear metallic behavior as shown in Fig. 4(c) which is a good indicator of the oxygen stoichiometry indicates that the oxygen content in our sample on LSAT could be beyond $SrCoO_{2.90}$ [42]. Thus it indeed represents the successful stabilization of Co^{4+} in our films on LSAT with $\delta = 0.1$, which is consistent with the most results reported previously [10,23]. The chemical shift in the cobalt L_3-edge between LSAT and LAO substrates is 0.37 eV. Since a shift of 1 eV in cobalt L_3-edge leads to the variation of $x = 1$ to $x = 0$ in $(La_{1-x}Sr_x)CoO_3$ system [43], the shift of 0.37 eV in our case gives rise to $\Delta\delta = 0.185$, associated with the transition from $SrCoO_{2.90}$ to $SrCoO_{2.72}$ with the strain varies from 1.0% to -1.0%. Identically, we estimated the $SrCoO_{2.835}$ films on STO substrate. A quantification of the oxygen content $3 - \delta$ is given in Fig. 2(b), which is obtained from cobalt L_3-edge XAS chemical peak shifts. It is clear that the oxygen concentration drops with the strain from 1.0% to 2.0% and –1.0%. It is then concluded that the epitaxial strain profoundly affects valence sates of cobalt cations and oxygen vacancies in the SCO films.

The valence states variation of cobalt cations and the oxygen vacancies evolution are supported by oxygen K-edge XAS measurements, as presented in Fig. 2(c). The oxygen K-edge XAS spectra were categorized into three regions of different hybrid structures,

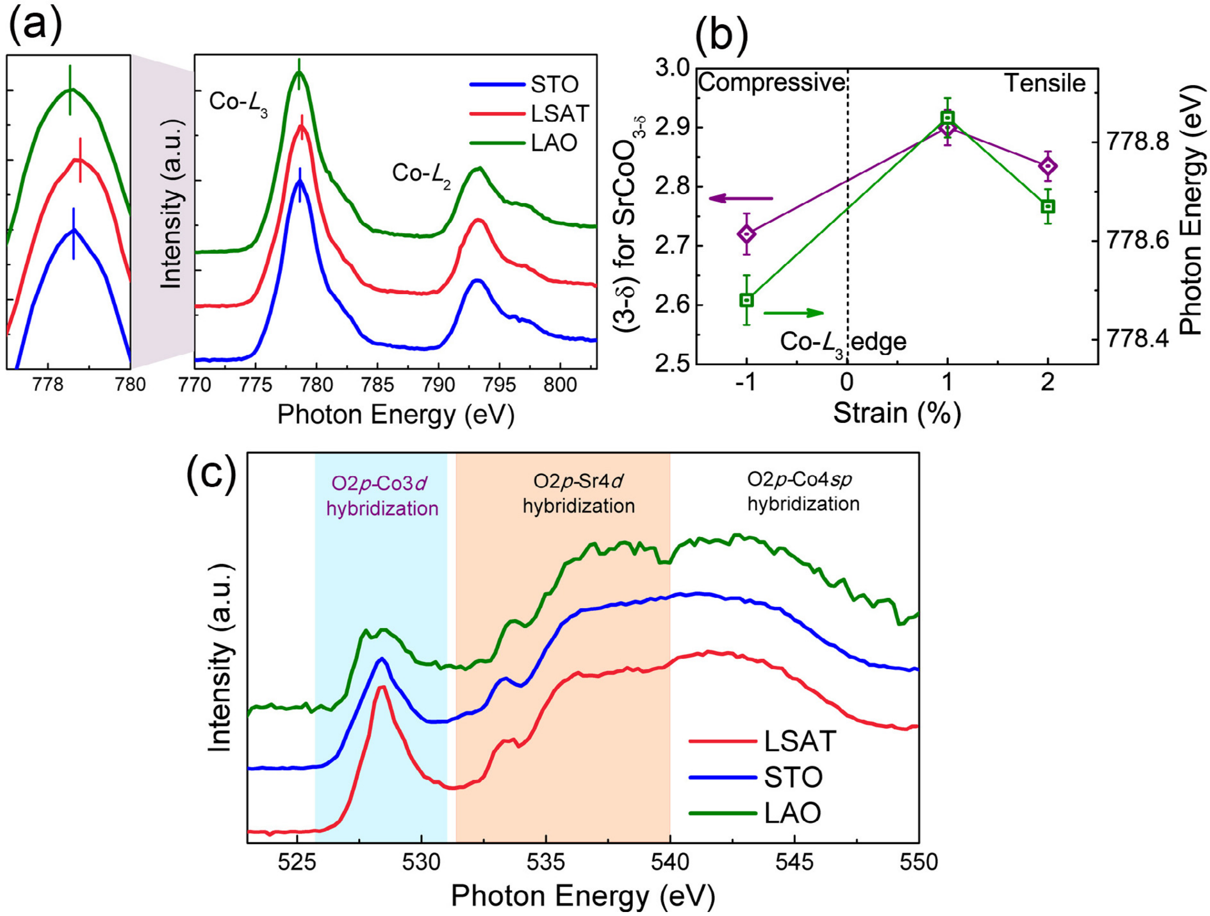

Fig. 2. Electronic structure variation and oxygen concentration changes probed by XAS. (a) Cobalt $L_{2,3}$-edge XAS curves of SCO films on LAO, LSAT and STO substrates. The two shoulders of the cobalt $L_{2,3}$-edge are denoted as Co-L_3 and Co-L_2, respectively. The left panel shows the enlarged cobalt $L_{2,3}$-edge XAS curves around cobalt L_3-edge. (b) Epitaxial strain dependent chemical shift of cobalt L_3-edge and oxygen concentration ($3 - \delta$ for SrCoO$_{3-\delta}$) variation. (c) Oxygen K-edge XAS curves of SCO films on LAO, LSAT and STO substrates.

which are linked to the empty O 2p states hybridizing with Co 3d, Sr 4d, and Co 4sp states, respectively [15,23,41]. The line shapes of the latter two regions were almost not changed under different strain states. On the contrary, the significant strain-dependent modification of line shape is observed in the O 2p-Co 3d hybridization peak, i.e., the so-called pre-edge peak, centered at ~528 eV (the left shadow area). The intensities of pre-edge peak show a systematic reduction with strains changing from 1.0% to 2.0% and -1.0%, suggesting the systematically increased oxygen vacancies in SCO films as the substrates varying from LSAT to STO and LAO, consistent with previous work [10,15,41].

Now, we address the question how orbital occupancy of the cobalt cations varies with the strain state of the SCO films. Cobalt $L_{2,3}$-edge XLD in Fig. 3, the normalized difference in absorption intensities of the XAS spectra from in-plane (E//ab) and out-of-plane (E//c) polarized soft X-rays, namely $I_{E//ab} - I_{E//c}$, could elucidate the differences in electronic occupancy of the cobalt 3d orbits [9]. The contribution of linearly polarized XAS signal at cobalt $L_{2,3}$-edge for t_{2g} (or e_g) band mainly arise from the unoccupied cobalt 3d xy (or $x^2 - y^2$) states by in-plane (E//ab) linearly polarized X-ray and xz/yz (or $3z^2 - r^2$) states by out-of-plane (E//c) linearly polarized X-ray. The configuration of the experimental setup is illustrated in Fig. 3(a). The polarization directions of the linearly polarized X-rays are tuned by rotating the X-ray incident angle, with 90° (left) and 30° (right) incident corresponding to in-plane (E//ab) and out-of-plane (E//c) polarization component, respectively. To analyze the cobalt $L_{2,3}$-edge XLD in a qualitative way, we used the linear dichroism sum rules. The integrated intensity contrast area under XLD spectra over the entire $L_{2,3}$ range (A_{XLD}; 700–803 eV) is related to the relative orbital occupancy between in-plane and out-of-plane oriented levels through the equation,

$$A_{XLD} = \frac{\int_{L_3+L_2} (I_{E//ab} - I_{E//c})dE}{\int_{L_3+L_2} (2I_{E//ab} + I_{E//c})dE} \tag{1}$$

For an isotropic orbital occupancy, the integrated intensity contrast A_{XLD} would be 0. However, for the anisotropy of orbital occupancy, the integrated area A_{XLD} should be proportional to the change in relative orbital occupancy between out-of-plane and in-plane oriented levels. That is, an increase of positive (negative) A_{XLD} area will have the larger occupancy of out-of-plane (in-plane) oriented orbitals. Fig. 3(b–d) show the normalized XAS and the concomitant XLD of the SCO films on LAO, LSAT and STO substrates, respectively. Upon exerting epitaxial strain on SCO films, different A_{XLD} values of 0.055, −0.015 and −0.022 for the strain from −1.0% to 1.0% and 2.0% are obtained as marked inside the figures, reflecting modulation of orbital occupancy of SCO by epitaxial strain (compressive and tensile). Notably, A_{XLD} is positive in the compressive strained state and negative in the tensile strained state. According to the acquired integrated results from Eq. (1), a preferential electron occupancy of out-of-plane oriented orbitals is favored in the films grown on compressive LAO substrate while the occupancy of in-plane oriented orbitals is favored for films on LSAT and STO substrates. Thus the epitaxial strain

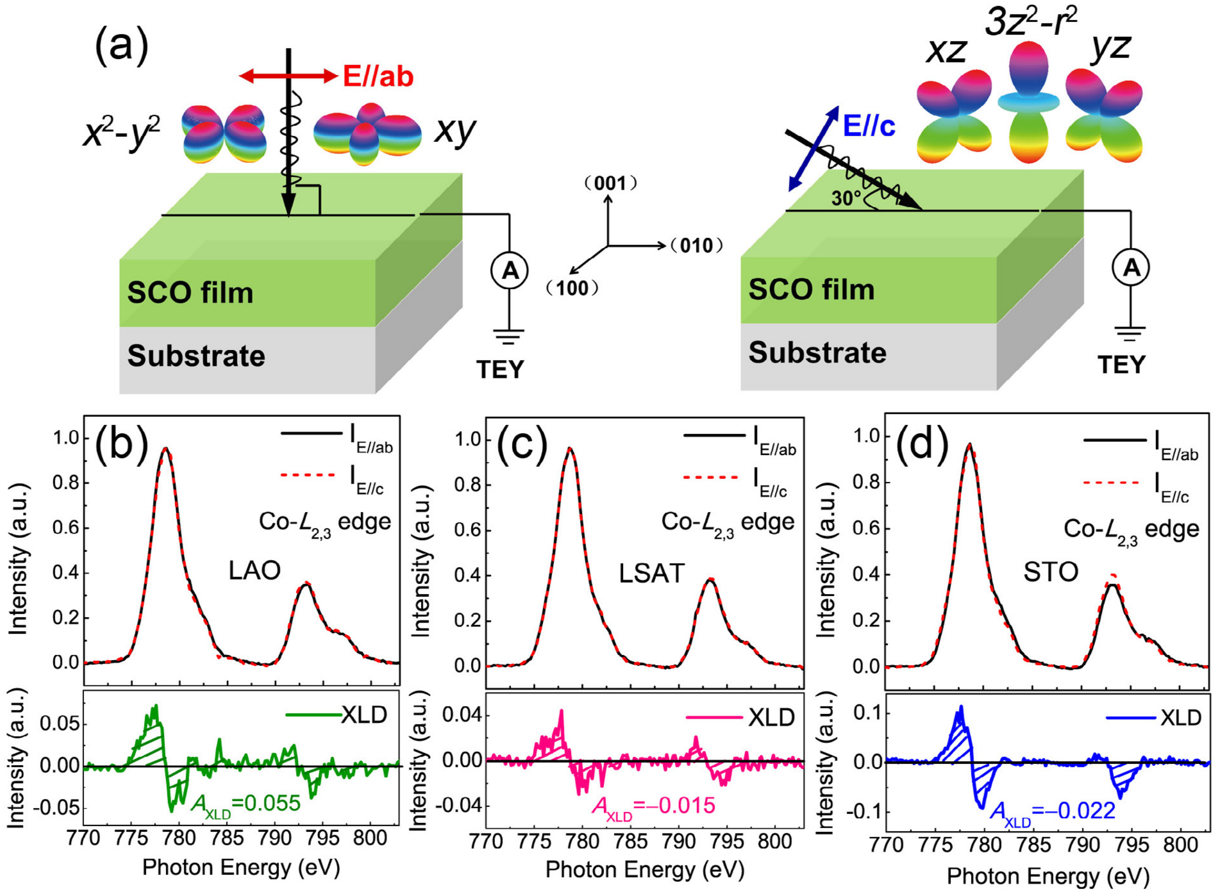

Fig. 3. Strain tuning of distinct orbital occupancy. (a) Schematic of experimental setup. In-plane (E//ab) and out-of-plane (E//c) linearly polarized X-rays were used to measure XAS of SCO films at cobalt $L_{2,3}$-edge with total electron yield (TEY) detection mode at room temperature. The contribution of linearly polarized XAS signal at cobalt $L_{2,3}$-edge for t_{2g} (or e_g) band mainly arise from the unoccupied cobalt 3*d* x^2-y^2 (or *xy*) states by in-plane E//ab and *xz*/*yz* (or $3z^2-r^2$) states by out-of-plane E//c. [E is the linear polarization vector of the photon]. The polarization directions of the linearly polarized X-rays are tuned by rotating the X-ray incident angle, with 90° (left) and 30° (right) incident corresponding to in-plane (E//ab) and out-of-plane (E//c) polarization component, respectively. Here the signal of XLD is defined as XLD = $(I_{E//ab} - I_{E//c})$. Normalized XAS and XLD of SCO films grown on LAO (b), LSAT (c) and STO (d) substrates. For clarity, the integrated intensity contrast A_{XLD} are directly marked inside the figures.

causes distinct orbital occupancy: larger occupancy of in-plane oriented orbits is favored for tensile strained SCO film, while larger occupancy of out-of-plane oriented orbitals is preferred once compressive strain is applied. It is interesting that the strain-dependence of orbital polarization measured for our SCO films is the same as that found in manganites [44,45].

The magnetic ordering and electrical transport properties should be sensitive to the variation in orbital occupancy and oxygen vacancies through strain. Fig. 4(a) presents magnetic hysteresis (*M*–*H*) loops of SCO films on various substrates. These *M*–*H* loops were measured at 10 K with in-plane magnetic fields (*H*). Magnetization-temperature (*M*–*T*) curves measured with *H* = 0.1 T are displayed in Fig. 4(b). At first glance, all coherently strained films show evidence of ferromagnetic order. However, it is interesting that 18 nm films on LSAT, which are under smaller tensile strain compared to films on STO, have the highest saturated magnetization of about 2.10 μ_B/Co and ferromagnetic transition temperature of about 175 K. By increasing the tensile strain by growth on STO, we find a lower saturated magnetization of about 0.86 μ_B/Co and Curie temperature of about 163 K. Remarkably, the films with compressive strain on LAO exhibit lowest saturated magnetization of about 0.70 μ_B/Co and Curie temperature of about 150 K than its tensile counterparts. Particularly, the saturated magnetization of SCO film on the LSAT is twice more than that of SCO film on the LAO. The robust magnetization means the stabilization of majority Co^{4+} in our SCO films, because the ferromagnetic to antiferromagnetic transition occurs at $\delta = 0.5$ with all Co^{3+} in BM-$SrCoO_{2.5}$ films [10,13,46]. The enhanced saturated magnetization in the tensile strained films compared to the compressive one indicates the critical role of epitaxial strain on the magnetic ordering of SCO films, which is consistent with the first principle calculations [12]. In P-SCO system, the Co^{4+} concentration is the main source of ferromagnetism [47]. As the concentration of the SCO film is approach to stoichiometric $SrCoO_3$, the Co^{4+} content is higher, accompanied by less oxygen vacancies, corresponding to the enhancement of saturated magnetization. It also implies that the −1% compressive strained SCO films on LAO substrate possess the lowest Co^{4+} concentration and the highest amounts of oxygen vacancies, followed by larger 2% tensile strained films on STO substrate, and finally the smaller 1% tensile strained films on LSAT substrate.

In addition to the magnetic ground states in these epitaxial films, we also observed an apparent difference in electrical transport properties of all films. As seen from the transport data in Fig. 4(c), a clear observation of metallic ground state in SCO films on LSAT indeed represents the successful stabilization of Co^{4+} in our films, as the insulator-to-metal transition occurs at $\delta \sim 0.1$ [16,42]. However, when the tensile strain is increased to 2%, the SCO films on STO are only metallic at temperatures above ∼215 K and then begin to exhibit insulating behavior. It implies that

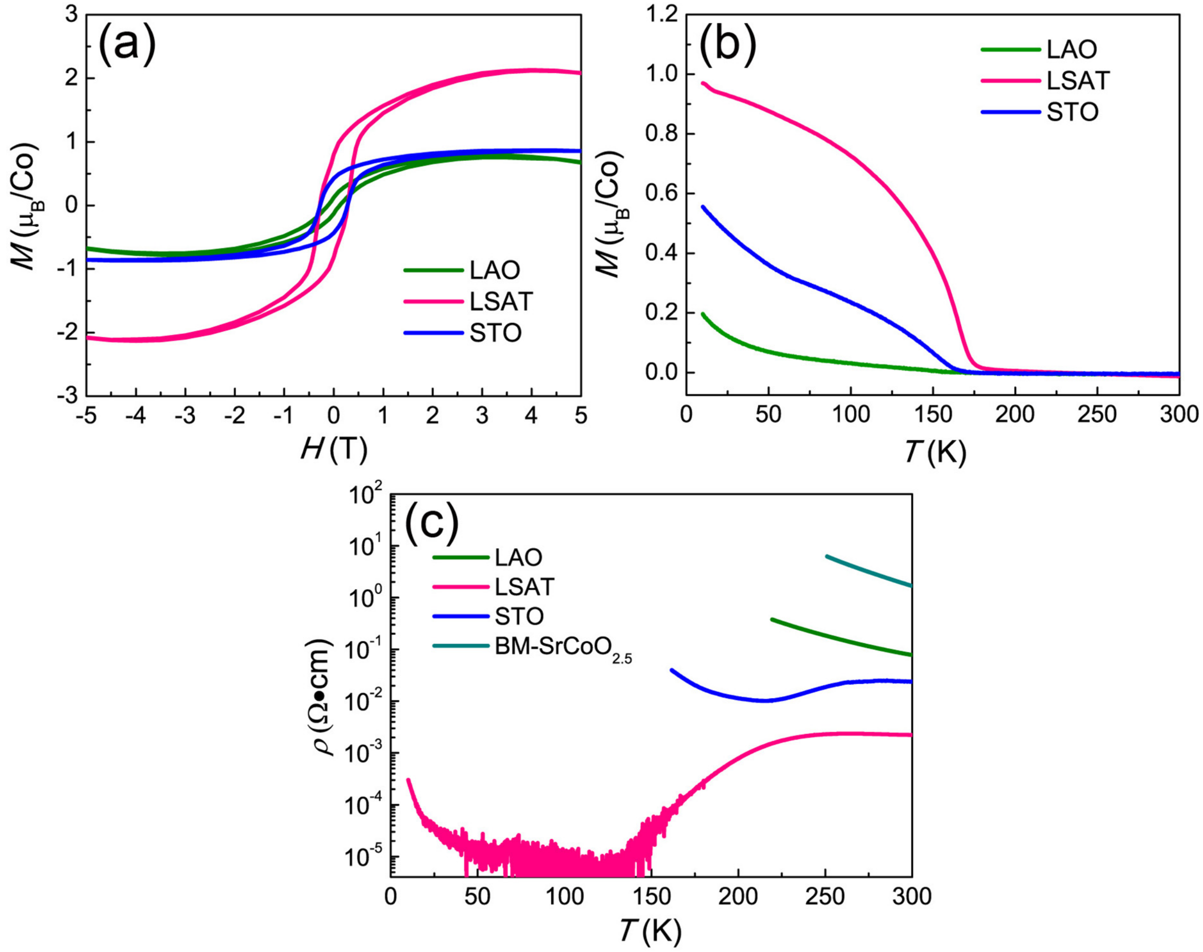

Fig. 4. Evolution of magnetic and transport properties with strains. (a) In-plane hysteresis loops at 10 K for SCO films on LAO, LSAT and STO substrates. (b) Temperature-dependent magnetization curves with field cooling, at a magnetic field strength of 0.1 T for three strained SCO films. (c) Temperature dependence of electrical resistivity (ρ) for SCO films on three substrates. As-grown BM-$SrCoO_{2.5}$ on STO is also included as a reference, putting an upper boundary on the oxygen deficiency for P-SCO.

the δ value of SCO films on STO is greater than 0.1 and that δ is increasing with such strain. Surprisingly, the SCO films on LAO are completely insulating when -1% compressive strain is applied. Of course, its resistivity is still at least two orders of magnitude lower than the highly insulating BM-$SrCoO_{2.5}$ ($\delta = 0.5$) films grown on STO with the same 18 nm thickness [Fig. 4(c)]. So the δ value of SCO films on LAO is still less than 0.5 but is greater than the value of SCO films on STO. These results clearly indicate the high sensitivity of electrical transport properties to changes in the oxygen content through strain. Combined with previous XAS and magnetization data, the estimated off-stoichiometric SCO phases of $SrCoO_{2.835}$, $SrCoO_{2.90}$, and $SrCoO_{2.72}$ on STO, LSAT, and LAO, respectively, were reasonable.

The magnetization, electrical transport properties and orbital occupancy measurements indicate different electronic structure of cobalt ions in the SCO films with the opposite strain. We then propose a possible spin states model in Fig. 5, in which the oxygen vacancies (V_O) are taken into account. Arrows represents the electrons in cobalt energy levels. For $3d^5$ configuration, the introduction of crystal and ligand fields split the Co-O molecular orbitals into the degenerated t_{2g} triplet and a degenerated e_g doublet with $xy/yz/xz$ and $x^2-y^2/3z^2-r^2$ symmetries [17]. As a result of the epitaxial strain, irrespective of tensile or compressive, t_{2g} and e_g orbital degeneracy would be further reduced. It is generally considered that the Co^{4+} ions are in IS state ($3d^5$: $t_{2g}^4e_g^1$) in P-SCO [16–18]. Recalling the results of the XAS measurements, magnetic and electrical properties, the SCO films grown on LSAT substrate possess lowest oxygen vacancies ($\delta \approx 0.1$, $SrCoO_{2.90}$) as well as highest saturated magnetization of about 2.10 μ_B/Co at 10 K, slightly smaller than the bulk value of 2.50 μ_B/Co with an IS sate [16] that can be attributed to tensile strain. The magnetization data indeed experimentally confirm the theoretically predicted IS state in SCO [17,18]. In this scenario, cobalt ions show the majority IS-Co^{4+} configuration ($3d^5$: $t_{2g}^4e_g^1$) with $S = 3/2$ in the 1% tensile strained films. Moreover, the spins prefer to occupy in-plane xy and x^2-y^2 orbits with lower orbital energy for t_{2g} and e_g, respectively (middle panel of Fig. 5), ascribed to the longer in-plane bond length [9]. Accordingly, holes take the orbits of degenerate yz and xz orbits, followed by the e_g orbits with higher energy level x^2-y^2 and $3z^2-r^2$. Note that epitaxial growth completely stoichiometric $SrCoO_3$ films is very arduous because energetic Co^{4+} ions prefer to convert to stable Co^{3+} ions. In order to be more rigorous and comprehensive, we still consider the presence of 20% Co^{3+} in SCO films on LSAT ($\delta \approx 0.1$, $SrCoO_{2.9}$). The pale yellow shade was used to guide the eyes (middle panel of Fig. 5). Here the Co^{3+} ions are completely antiferromagnetic with high spin state (BM-$SrCo^{3+}O_{2.5}$ is an antiferromagnet with the Néel temperature of 570 K and the magnetic structure is G-type in which near-neighboring Co^{3+} ions are in high spin state ($3d^6$: $t_{2g}^4e_g^2$, $S = 2$) but have always opposite spins, Refs. [46,48–50]).

It should be noted that HS state Co^{3+} ions have full filling e_g orbits, as shown in Fig. 5, so the strain effect has negligible influence on orbital occupancy in the e_g orbitals between films on LSAT and STO and films on LAO. However, strain effect will result in

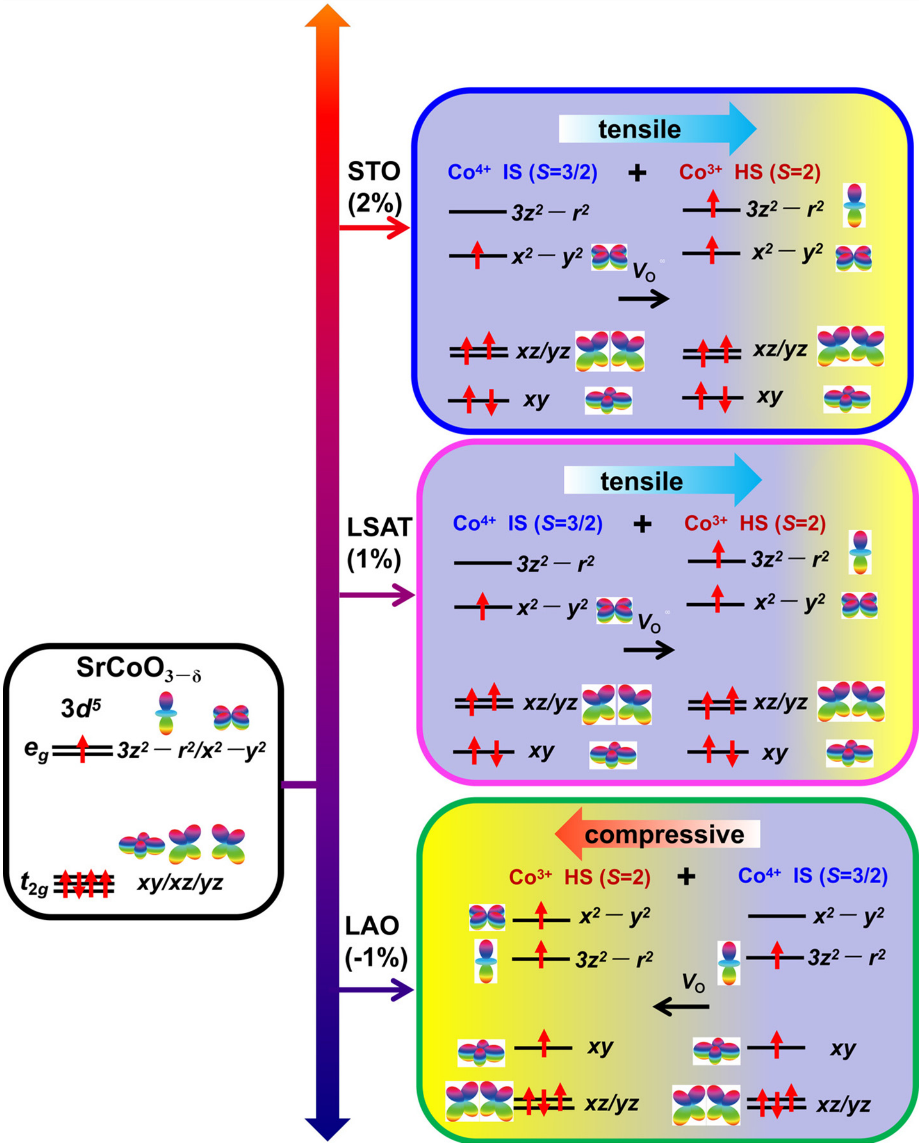

Fig. 5. Spin states model. A schematic of electron and orbital configurations of the cobalt 3*d* band associated with growth SCO films on tensile LSAT and STO substrates and on compressive LAO substrate showing coupled IS-Co^{4+}/HS-Co^{3+} states in different proportions depending on strain states. Arrows represent electrons in cobalt energy level. The percentages of strain induced by the different substrates on SCO films are indicated along the vertical arrow on the left of the figure. Respectively, representing the IS-Co^{4+} and HS-Co^{3+} contents of pale blue and pale yellow shadows are marked on the right side of the figure, which is used to guided the eyes. (For interpretation of the references to colour in this figure legend, the reader is referred to the web version of this article.)

some differences in the t_{2g} orbitals because there are unoccupied t_{2g} orbitals. When films are in tensile strain on LSAT and STO, in the t_{2g} orbitals this results in a higher energy for the degenerate out-of-plane *xz* and *yz* orbits, compared to films on LAO. Electrons in the t_{2g} shell in the films on STO and LSAT prefer to fully occupy the lower energy in-plane *xy* orbitals leaving holes in degenerate out-of-plane *xz* and *yz* orbits, while in contrast the holes in films on LAO occupy nondegenerate in-plane *xy* orbitals [9]. This contrast in hole density between tensile strained SCO films on STO and LSAT and compressive strained films on LAO is also consistent with our XLD measurements shown in Fig. 3. Of course, different ratio of Co^{3+} to Co^{4+} in these three type films will have corresponding contribution to XLD.

The ferromagnetic phase of P-SCO is currently attributed to the double exchange interaction between hybridized 3*d* states in cobalt ions [17,18,36,37,51]. Films on STO show ferromagnetic ordering most likely through the similar double exchange mechanism with on LSAT, but in the case of STO the saturated magnetization at 10 K only about 0.86 μ_B/Co. XAS, magnetization and transport data have shown that the oxygen vacancy contents of these SCO films on LSAT and STO are different due to the changes in strain. The lower magnetization and increased oxygen vacancy content of films on STO suggest an increased presence of HS-Co^{3+} of 33% ($\delta \approx 0.165$, $SrCoO_{2.835}$). The concomitant electron and orbital configurations of the cobalt 3*d* band associated with a mixture of IS-Co^{4+} and HS-Co^{3+} states were presented in the top panel of Fig. 5.

The situation turns out to be dramatically different for the films with − 1% compressive strain, where the most amounts of oxygen vacancies exist ($\delta \approx 0.28$, $SrCoO_{2.72}$). It is worth noting that SCO films on LAO substrate with $\delta \approx 0.28$ almost deviate from P-SCO ($0 \leq \delta \leq 0.25$) because of containing a considerable amount of oxygen vacancies. It is also directly corroborated by HADDF-STEM image of Fig. 1(b). The film was almost transformed into BM-$SrCoO_{2.5}$ phase except for a few atomic unit cells between the two white lines remaining P-SCO phase [Fig. 1(b)]. Of course, we cannot completely rule out the possibility of long-time transmission electron microscopy sample preparation and argon ion bombardment makes the oxygen vacancies enhanced. Hence HS state-Co^{3+} ($3d^6$: $t_{2g}^4e_g^2$, $S = 2$) emerges in the samples [46]. Note that the compressive strained films also show clear magnetization (Fig. 4), indicating IS-Co^{4+} ions remain besides the HS-Co^{3+} configuration. These two spin states couple together, which is schematically illustrated in the bottom panel of Fig. 5. The full filling e_g orbits plus the holes in the t_{2g} orbits in the film on LAO occupy the nondegenerate xy level for HS-Co^{3+}, together with the preferred occupied out-of-plane orbits for IS-Co^{4+} well elucidate the fact that out-of-plane orbital occupancy are still favored under the compressive strain.

The present results verify the controllable oxygen vacancies, orbital occupancy and magnetic transition through the facile application of epitaxial strain, both tensile and compressive, in strontium cobaltite similar to manganites. However, the interplay between four degrees of freedom in strontium cobaltite, especially the orbital occupancy and magnetic ordering still needs to be identified. Based on the spin states model proposed above, we can get a reasonable explanation for the magnetic properties of SCO films under tensile and compressive strains. As mentioned before, the ferromagnetic phase of P-SCO is attributed to the double exchange interaction between hybridized $3d$ states in cobalt ions [17,18,36,37,51]. Our orbital occupancy analysis has revealed the favored in-plane oriented orbits under tensile strain. The strong bonding anisotropy oriented within in-plane improves the hybridization between in-plane electrons and oxygen atoms, thus promotes the double exchange. Compared to tensile strain, the preferential out-of-plane oriented orbital occupancy plus the largest amounts of oxygen vacancies under the compressive strain evidently weakens the double exchange, thus worsens the magnetic properties of SCO films. So our results presented here give an direct experimental evidence for the existence of strong coupling between lattice (epitaxial strain), charge (the changes of valence states of cobalt cations induced by oxygen vacancies), spin (magnetization) and orbit (orbital occupancy) in complex oxide of strontium cobaltite, which provides useful information for developing novel and efficient spintronics, catalytic, and electrochemical devices by the precise control of oxygen vacancies using epitaxial strain.

4. Conclusions

To conclude, it is experimentally demonstrated that the oxygen vacancies are greatly enhanced as the strain changes from smaller tensile 1.0% to larger tensile 2.0%, then moderate compressive -1.0% in $SrCoO_{3-\delta}$ films, associated with $3-\delta$ varying from $\sim$2.90 to $\sim$2.835, then to $\sim$2.72. The favored in-plane orbital occupancy for tensile strained film and out-of-plane orbital occupancy for the compressive state correspond to coupled IS-Co^{4+}/HS-Co^{3+} spin configurations in different proportions depending on strain states, bring about robust magnetization in tensile strained $SrCoO_{3-\delta}$ than the compressive counterparts. The experimental results further prove the existence of strong coupling between the lattice, charge, spin and orbital degrees of freedom in complex oxide of strontium cobaltite. Meanwhile, we provide a nostrum for designing and controlling new ionically active properties via strain-engineered oxygen vacancies in strong correlated transition-metal oxides.

Acknowledgements

The authors acknowledge Beamline BL08U1A in Shanghai Synchrotron Radiation Facility (SSRF) for XAS and XLD measurements. This work was supported by the National Natural Science Foundation of China (Grant Nos. 51671110, 51571128, 51590883 and 51771198) and National Key Research and Development Program (Grant Nos. 2016YFA0203800 and 2016YFA0300701).

References

[1] E. Dagotto, Science 309 (2005) 257.
[2] Y.D. Chuang, A.D. Gromko, D.S. Dessau, T. Kimura, Y. Tokura, Science 292 (2001) 1509.
[3] E. Dagotto, Rev. Mod. Phys. 66 (1994) 763.
[4] S.V. Kalinin, N.A. Spaldin, Science 341 (2013) 858.
[5] S.V. Kalinin, A. Borisevich, D. Fong, ACS Nano 6 (2012) 10423.
[6] C. Becher, L. Maurel, U. Aschauer, M. Lilienblum, C. Magén, D. Meier, E. Langenberg, M. Trassin, J. Blasco, I.P. Krug, P.A. Algarabel, N.A. Spaldin, J.A. Pardo, M. Fiebig, Nat. Nanotechnol. 10 (2015) 661.
[7] F. Wang, Y.Q. Zhang, Y. Bai, W. Liu, H.R. Zhang, W.Y. Wang, S.K. Li, S. Ma, X.G. Zhao, J.R. Sun, Z.H. Wang, Z.J. Wang, Z.D. Zhang, Appl. Phys. Lett. 109 (2016) 052403.
[8] W. Li, R. Zhao, L. Wang, R. Tang, Y. Zhu, J.H. Lee, H. Cao, T. Cai, H. Guo, C. Wang, L. Ling, L. Pi, K. Jin, Y. Zhang, H. Wang, Y. Wang, S. Ju, H. Yang, Sci. Rep. 3 (2013) 2618.
[9] V.V. Mehta, N. Biskup, C. Jenkins, E. Arenholz, M. Varela, Y. Suzuki, Phys. Rev. B 91 (2015) 144418.
[10] H. Jeen, W.S. Choi, M.D. Biegalski, C.M. Folkman, I.-C. Tung, D.D. Fong, J.W. Freeland, D. Shin, H. Ohta, M.F. Chisholm, H.N. Lee, Nat. Mater. 12 (2013) 1057.
[11] H. Jeen, W.S. Choi, J.W. Freeland, H. Ohta, C.U. Jung, H.N. Lee, Adv. Mater. 25 (2013) 3651.
[12] J.H. Lee, K.M. Rabe, Phys. Rev. Lett. 107 (2011) 067601.
[13] C.K. Xie, Y.F. Nie, B.O. Wells, J.I. Budnick, W.A. Hines, B. Dabrowski, Appl. Phys. Lett. 99 (2011) 052503.
[14] R.L. Toquin, W. Paulus, A. Cousson, C. Prestipino, C. Lamberti, J. Am. Chem. Soc. 128 (2006) 13161.
[15] N. Lu, P. Zhang, Q. Zhang, R. Qiao, Q. He, H.-B. Li, Y. Wang, J. Guo, D. Zhang, Z. Duan, Z. Li, M. Wang, S. Yang, M. Yan, E. Arenholz, S. Zhou, W. Yang, L. Gu, C.-W. Nan, J. Wu, Y. Tokura, P. Yu, Nature 546 (2017) 124.
[16] Y. Long, Y. Kaneko, S. Ishiwata, Y. Taguchi, Y. Tokura, J. Phys.: Condens. Matter 23 (2011) 245601.
[17] R.H. Potze, G.A. Sawatzky, M. Abbate, Phys. Rev. B 51 (1995) 11501.
[18] M. Zhuang, W. Zhang, A. Hu, N. Ming, Phys. Rev. B 57 (1998) 13655.
[19] Q. Lu, B. Yildiz, Nano Lett. 16 (2016) 1186.
[20] A. Nemudry, P. Rudolf, R. Schöllhorn, Chem. Mater. 8 (1996) 2232.
[21] S.J. Callori, S. Hu, J. Bertinshaw, Z.J. Yue, S. Danilkin, X.L. Wang, V. Nagarajan, F. Klose, J. Seidel, C. Ulrich, Phys. Rev. B 91 (2015) 140405(R).
[22] S. Hu, Z. Yue, J.S. Lim, S.J. Callori, J. Bertinshaw, A. Ikeda-Ohno, T. Ohkochi, C.-H. Yang, X. Wang, C. Ulrich, J. Seidel, Adv. Mater. Interfaces 2 (2015) 1500012.
[23] J.R. Petrie, C. Mitra, H. Jeen, W.S. Choi, T.L. Meyer, F.A. Reboredo, J.W. Freeland, G. Eres, H.N. Lee, Adv. Funct. Mater. 26 (2016) 1564.
[24] P. Agrawal, J. Guo, P. Yu, C. Hébert, D. Passerone, R. Erni, M.D. Rosell, Phys. Rev. B 94 (2016) 104101.
[25] U. Aschauer, R. Pfenninger, S.M. Selbach, T. Grande, N.A. Spaldin, Phys. Rev. B 88 (2013) 054111.
[26] R.U. Chandrasena, W. Yang, Q. Lei, M.U. Delgado-Jaime, K.D. Wijesekara, M. Golalikhani, B.A. Davidson, E. Arenholz, K. Kobayashi, M. Kobata, F.M.F. de Groot, U. Aschauer, N.A. Spaldin, X. Xi, A.X. Gray, Nano Lett. 17 (2017) 794.
[27] S.-Y. Choi, S.-D. Kim, M. Choi, H.-S. Lee, J. Ryu, N. Shibata, T. Mizoguchi, E. Tochigi, T. Yamamoto, S.-J.L. Kang, Y. Ikuhara, Nano Lett. 15 (2015) 4129.
[28] R.L. Johnson-Wilke, D. Marincel, S. Zhu, M.P. Warusawithana, A. Hatt, J. Sayre, K.T. Delaney, R. Engel-Herbert, C.M. Schlepütz, J.-W. Kim, V. Gopalan, N.A. Spaldin, D.G. Schlom, P.J. Ryan, S. Trolier-McKinstry, Phys. Rev. B 88 (2013) 174101.
[29] S. Hu, Y. Wang, C. Cazorla, J. Seidel, Chem. Mater. 29 (2017) 708.
[30] C. Cazorla, Phys. Rev. Appl. 7 (2017) 044025.
[31] J.H. Lee, K.M. Rabe, Phys. Rev. B 84 (2011) 104440.
[32] Y. Tokura, N. Nagaosa, Science 288 (2000) 462.
[33] B. Cui, C. Song, H. Mao, H. Wu, F. Li, J. Peng, G. Wang, F. Zeng, F. Pan, Adv. Mater. 27 (2015) 6651.
[34] J. Liu, M. Kareev, D. Meyers, B. Gray, P. Ryan, J.W. Freeland, J. Chakhalian, Phys. Rev. Lett. 109 (2012) 107402.
[35] A. Frano, E. Schierle, M.W. Haverkort, Y. Lu, M. Wu, S. Blanco-Canosa, U. Nwankwo, A.V. Boris, P. Wochner, G. Cristiani, H.U. Habermeier, G. Logvenov, V. Hinkov, E. Benckiser, E. Weschke, B. Keimer, Phys. Rev. Lett. 111 (2013) 106804.
[36] J. Kuneš, V. Křápek, N. Parragh, G. Sangiovanni, A. Toschi, A.V. Kozhevnikov, Phys. Rev. Lett. 109 (2012) 117206.
[37] J.-Y. Yang, C. Terakura, M. Medarde, J.S. White, D. Sheptyakov, X.-Z. Yan, N.-N. Li, W.-G. Yang, H.-L. Xia, J.-H. Dai, Y.-Y. Yin, Y.-Y. Jiao, J.-G. Cheng, Y.-L. Bu, Q.-F. Zhang, X.-D. Li, C.-Q. Jin, Y. Taguchi, Y. Tokura, Y.-W. Long, Phys. Rev. B 92 (2015) 195147.
[38] A. Kovács, R. Schierholz, K. Tillmann, J. Large-Scale Res. Facil. 2 (2016) A43.
[39] O. Vlašín, R. Jarrier, R. Arras, L. Calmels, B. Warot-Fonrose, C. Marcelot, M. Jamet, P. Ohresser, F. Scheurer, R. Hertel, G. Herranz, S. Cherifi-Hertel, ACS Appl. Mater. Interfaces 8 (2016) 7553.

[40] V.R. Singh, K. Ishigami, V.K. Verma, G. Shibata, Y. Yamazaki, T. Kataoka, A. Fujimori, F.-H. Chang, D.-J. Huang, H.-J. Lin, C.T. Chen, Y. Yamada, T. Fukumura, M. Kawasaki, Appl. Phys. Lett. 100 (2012) 242404.

[41] L. Karvonen, M. Valkeapää, R.-S. Liu, J.-M. Chen, H. Yamauchi, M. Karppinen, Chem. Mater. 22 (2010) 70.

[42] S. Balamurugan, K. Yamaura, A.B. Karki, D.P. Young, M. Arai, E. Takayama-Muromachi, Phys. Rev. B 74 (2006) 172406.

[43] Z. Hu, C. Grazioli, M. Knupfer, M.S. Golden, J. Fink, P. Mahadevan, A. Kumar, S. Ray, D.D. Sarma, S.A. Warda, D. Reinen, S. Kawasaki, M. Takano, C. Schüssler-Langeheine, C. Mazumdar, G. Kaindl, J. Alloys Compd. 343 (2002) 5.

[44] Y. Konishi, Z. Fang, M. Izumi, T. Manako, M. Kasai, H. Kuwahara, M. Kawasaki, K. Terakura, Y. Tokura, J. Phys. Soc. Jpn. 68 (1999) 3790.

[45] C. Aruta, G. Ghiringhelli, A. Tebano, N.G. Boggio, N.B. Brookes, P.G. Medaglia, G. Balestrino, Phys. Rev. B 73 (2006) 235121.

[46] T. Takeda, Y. Yamaguchi, H. Watanabe, J. Phys. Soc. Jpn. 33 (1972) 970.

[47] H. Taguchi, M. Shimada, M. Koizumi, J. Solid State Chem. 29 (1979) 221.

[48] T. Takeda, H. Watanabe, J. Phys. Soc. Jpn. 33 (1972) 973.

[49] A. Muñoz, C. de la Calle, J.A. Alonso, P.M. Botta, V. Pardo, D. Baldomir, J. Rivas, Phys. Rev. B 78 (2008) 054404.

[50] B. Cui, F. Li, C. Song, J.J. Peng, M.S. Saleem, Y.D. Gu, S.N. Li, K.L. Wang, F. Pan, Phys. Rev. B 94 (2016) 134403.

[51] W.S. Choi, H. Jeen, J.H. Lee, S.S. Ambrose Seo, V.R. Cooper, K.M. Rabe, H.N. Lee, Phys. Rev. Lett. 111 (2013) 097401.